Journal of Non-Crystalline Solids 524 (2019) 119656

Contents lists available at ScienceDirect

Journal of Non-Crystalline Solids

journal homepage: www.elsevier.com/locate/jnoncrysol

Amorphous boron arsenide

Murat Durandurdu

Department of Materials Science & Nanotechnology Engineering, Abdullah Gül University, Kayseri 38039, Turkey

ARTICLE INFO

Keywords:
Amorphous
Boron arsenide
Metallization

ABSTRACT

The short-range order and electrical properties of amorphous boron arsenide (BAs) are evaluated by means of ab initio molecular dynamics simulations. The amorphous model is obtained from the fast solidification of the BAs melt and consists of B-rich and As-rich domains. The average coordination number of B- and As-atoms are found as 4.97 and 3.34, respectively. B-atoms have a tendency to form pentagonal pyramidal-like configurations as commonly seen in boron or boron rich materials. Yet B_{12} molecules do not develop in the system but the formation of a B_{10} cluster is perceived in the network. On the other hand, As-atoms have a trend to structure chain-like motifs and four-membered rings. Amorphization yield about 31% volume expansion in the amorphous network. All these findings reveal that the model shows strong chemical disorder and its short-range order is considerably different than that of the crystal. Amorphization-induced metallization is proposed for BAs.

1. Introduction

Boron Arsenide (BAs), a member of the III–V semiconductor family, was first synthesized in 1958 [1]. It has the cubic zinc blende (ZB) crystal having lattice parameter of 4.777 Å. BAs is the most covalent III-V material having the lowest Phillips iconicity $f_i = 0.002$ [2]. This feature is due to the lack of *p* electrons in the core of B atom and its small size [3]. The reservation of cation and anion roles is observed for BAs.

The difficulties to synthesize BAs have limited experimental studies on this material. Therefore, its properties have not been fully discovered yet. At present, perhaps the most remarkable feature of BAs revealed is its high thermal conductivity [4]. Also BAs is considered as a potential candidate for photovoltaic and photo- electrochemical applications [5]. Some theoretical investigations have been carried out to better understand this material and estimate its elastic [6–11], the electronic [12–17] and the optical properties [18,19].

The high-pressure behavior of BAs has been investigated both experimentally and theoretically. Since the ZB structured materials commonly transform to a rocksalt structure (RS) with the application of pressure, the RS phase has been considered as a possible candidate for BAs as well in the theoretical studies. The ZB-to-RS phase change was predicted to occur at 93–141 GPa in theoretical examinations [3,6,16,20,21]. On the other hand, the experimental investigation [22] could not verify this phase transition and instead reported the amorphization of BAs at a pressure of 125 GPa. The amorphous phase persevered to up to 165 GPa and could be quenchable to the ambient pressure. To our knowledge no other experimental investigation has been performed to validate the pressure-induced amorphization in BAs so far.

Experimental studies also reported an amorphous form of BAs. The films deposited on silicon substrates using the thermal decomposition of a diborane arsine mixture in hydrogen atmosphere at 800–850 °C were found to be amorphous [23]. Yet to date its atomic structure has not been investigated, to our knowledge. The main purpose of present simulation is to generate an amorphous BAs model and reveal its structural and electiricl properties in details. Our simulations disclose that the amorphous form has a local structure, considerably different from that of the crystal and such structural differences yields metallization in BAs.

2. Method

An ab initio code, SIESTA [24], within the pseudopotential method [25] and a generalized gradient approximation [26,27] was used in this study to generate an amorphous model. Double-zeta (DZ) basis functions were employed for the molecular dynamics (MD) simulations whereas double-zeta plus polarization (DZP) basis sets were employed for geometry optimization. The Brillouin zone sampling was performed at Γ point. We executed the NPT-MD calculations with a time step of 1.0 fs. The initial structure was chosen to be the ZB crystal consisting of 216 atoms. The ZB phase was exposed to 5500 K for 2.0 ps. The resulting structure was quickly cooled down to 3500 K. We then equilibrated the structure at 3500 K for 20 ps. After then, temperature was decreased to 2500 K at which point the structure was equilibrated again for 20.0 ps. This was followed by quenching to 300 K over a time period

E-mail address: murat.durandurdu@agu.edu.tr.

https://doi.org/10.1016/j.jnoncrysol.2019.119656
Received 4 July 2019; Received in revised form 25 August 2019; Accepted 26 August 2019
Available online 06 September 2019

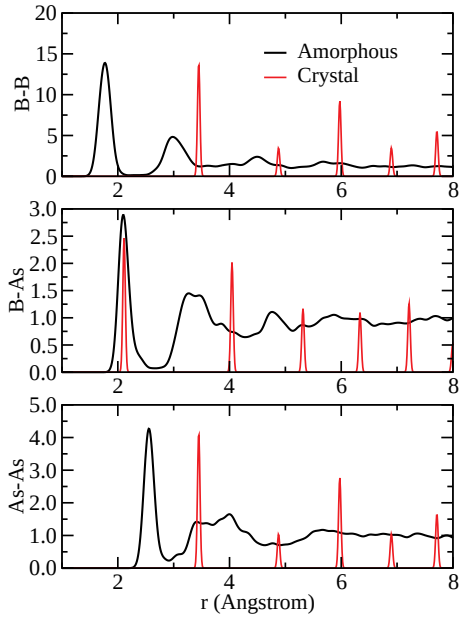

Fig. 1. The B—B, B—As and As—As pair correlation functions. For clarity, the intensity of pair correlation functions of the crystal is scaled.

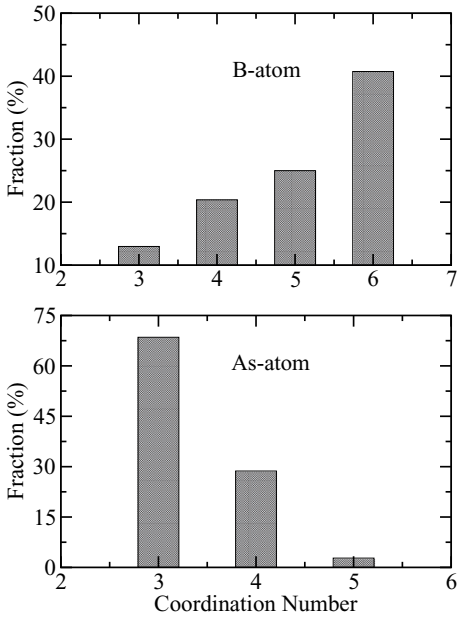

Fig. 2. Coordination distribution of B and As atoms.

of about 100 ps. Finally the system was relaxed using the maximum atomic force criteria of 0.01 eV/Å. The ISAACS [28] program was used attain some structural information (chemical identities, coordination numbers, coordination distribution etc.) about the amorphous system at the atomistic level. The VESTA [29] program was used to visualize the amorphous model and clusters formed in the network.

3. Results

We start our examination on the microstructure and the bonding character of each species using two-body partial pair correlation functions and three-body bond angle correlation functions. Both correlation functions provide substantial information about the nature of the local structure of the network. For the amorphous and crystalline configurations, we consider three partial pair correlations of the components: B—B, B—As and As—As and provide them in Fig. 1. From the figure, one can see the drastic structural difference between amorphous and the crystalline phases. Namely the As—As and B—B homopolar bonds do not exist in the crystalline phase but such bonds exist in the amorphous network as indicated by the peaks appeared at around 1.77 Å (B—B correlation) and 2.55 Å (for the As—As correlations). The finding indicates the presence of strong chemical disorder in the network. The first three peaks of the B—B pair are positioned at approximately 1.77 Å, 2.98 Å and 4.49 Å, respectively. These values are quite comparable with the experimental values of 1.80 Å, 2.93 Å, and 4.38 Å reported for amorphous B [30], 1.802 (1.803) Å, 2.99 (3.03) Å and 4.31 (4.56) Å stated for α- (β-) rhombohedral boron crystal [31], and 1.76 Å, 3.15 Å, and 4.7 Å found for liquid B [32]. The pronounced B—B peaks at 2.98 Å and 4.49 Å peaks were also observed in the amorphous B and liquid B (see Fig. 4 of Ref. 31). They are a result of pentagonal pyramid-like configurations as will be discussed in details below. All these findings suggest that B—B clusters formed amorphous BAs are similar to those of pure B systems (crystals, amorphous or liquid). The As—As bonding results in a peak at 2.55 Å, which are fairly close to the experimental results of 2.49 Å (X-Ray) [33], 2.51 Å (neutron) [34] reported amorphous As and 2.52 Å in the rhombohedral A7 crystal and 2.54 Å in the liquid As [35]. The B—As first maximum peak of the noncrystalline state is located at around 2.10 Å, well overlap with 2.10 Å in the crystal. The evaluation of the peak intensity of all pairs proposes that the amorphous configuration is dominated by chemical disorder.

More information regarding the short-range order can be acquired by examining the coordination, coordination distribution and chemical environment of B and As atoms. For this purpose, we use the position of the first minimum from partial correlation functions as the cutoff radii to define the first coordination shells. Particularly, the B—As, B—B and As—As nearest neighbor cutoffs are set to be 2.52, 2.17, and 2.94 Å, respectively. Fig. 2 shows the coordination distribution of each species. B atoms have coordination ranging from three to six. The sixfold coordination is the most dominant one with a frequency of 40.7%. The fraction of threefold, fourfold and fivefold coordination numbers is about 13.0, 20.0 and 25.0%, correspondingly. The average B—B and B—As coordination numbers are 3.87 and 1.10, respectively, which lead to the total coordination number of B atoms to be about 4.97. This finding means that B-atoms have a strong tendency to form wrong bonds (B—B bonds). For the case of As atoms, the coordination ranges from two to four and the threefold coordination is the leading one with a frequency of about 69%. The mean As—As and As—B coordination is 2.24 and 1.10, respectively, which yield the total coordination of As atoms to be 3.34. So one can see that As-atoms also have an affinity to form homopolar (As—As) bonds. These findings show that the total coordination severally deviates from the ideal tetrahedral coordination and the microstructure of amorphous network differs from that of the ZB crystal.

The chemical distribution examination given in Table 1 provides more knowledge about the microstructure of the amorphous configuration. The crystalline structure is contracted by only B—As_4 and As—B_4 type motifs. Such motifs, however, are not visibly presented in the noncrsytalline state, revealing, again, drastic structural differences between these two forms of BAs. B—B_6 (20.37%), B-B_5As (17.59%) and B-B_4As (12.96%) are the most dominated clusters around B-atoms. On the other hand As—As_3 (39%), As-BAs_2 (24%) and As-B_2As_2 (12%) are the most privilege ones for As-atoms. These findings suggest the occurrence of B-rich and As rich regions in the network, which is also confirmed by the visualizing the model provided in Fig. 3.

The Voronoi polyhedron technique can shed some additional lights on the local structure of the model. A Voronoi cluster is expressed by the indices $< k_3, k_4, k_5, k_6, \ldots >$, here k_i is the number of i-edge faces of a motif and Σk_i is coordination number. We find that about 35% of B atoms present the < 2,2,2,0 > index that is the pentagonal pyramid-like motif (Fig. 4). This means that almost all sixfold coordinated

Table 1
Chemical identities around B and As atoms for amorphous configuration.

B		As	
B_6	20.37%	As_3	36.11%
B_5As	17.59%	B_1As_2	22.22%
B_4 As	12.96%	B_2As_2	11.11%
B_2As	8.333%	B_2As	8.333%
BAs_3	6.481%	B_3As	7.407%
B_3As_2	6.481%	B_1As_3	6.481%
B_2As_2	6.481%	As_4	2.778%
B_5	3.704%	B_3	1.852%
B_3As	3.704%	B_4	0.926%
B_4As_2	2.778%	B_5	0.926%
B_3	2.778%	B_4As	0.926%
B_4	1.852%	B_5As	0.926%
As_4	1.852%		
BAs_2	1.852%		
B_2As_3	1.852%		

configuration form the pentagonal pyramid-like motif in the amorphous network. The < 2,3,0,0 > type clusters corresponding incomplete pentagonal pyramid-like polyhedrons are also presented in the model. Their frequency is about 22%. We should noted here that the pentagonal pyramid is the main building unit of B_{12} molecules and hence B and B-rich crystals/amorphous materials. Yet we do not see the formation of a complete B_{12} cluster in the model but we observe for the first time the formation of a B_{10} molecule (Fig. 4) in an amorphous model. Based on this finding, we propose that B-atoms have a tendency to form a local structure similar to B- or B-rich crystalline/amorphous materials.

We provide the bond angle distributions for the B-and As-centered angles in Fig. 5. The crystal has only As-B-As and B-As-B angles at the ideal tetrahedral angle of ~109.5°. In the amorphous network, As-B-As angles produce a peak at around 107.7° close to the tetrahedral angle. On the other hand, the B-As-B distribution has three main peaks at 50°, 90° and 105°. As-centered atoms that have a tendency to form pentagonal-like pyramids and bond(s) with only B atoms produce such angles. The As-As-As angles yields a peak located at around 104°, which are indeed close to 97° formed in the A7. The main B-B-B peaks are at 60° and 108° and subpeaks are at 120° and 130°. The first two angles are due to the intra-pentagonal pyramid-like motifs' bonds while the others are a result of the inter-pentagonal pyramid-like clusters' bonds.

We finally calculate the total electron density of states (TDOS) to reveal the electronic properties of amorphous BAs. For the comparison purpose, the TDOS of the ZB structured crystal is also calculated and presented in Fig. 6. The band gap energy of the crystal is estimated as 1.67 eV, which is in agreement with experimental results of 1.4–1.77 eV [5,36–38] and theoretical (including GW calculations) data of 1.58–2.04 eV [10,39–43]. On the other hand, for the amorphous

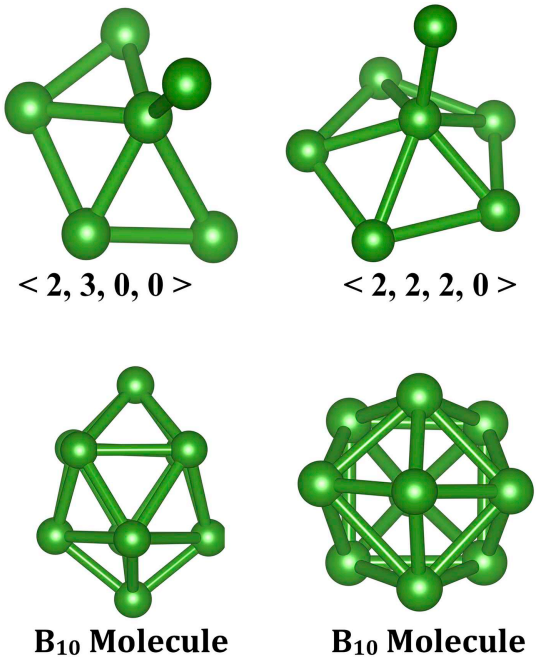

Fig. 4. The pentagonal pyramid-like motif and B10 molecule formed in the BAs amorphous model.

configuration, it is indeed hard to conclude its electronic structure since its TDOS does present a semi-metallic-like band structure. From the inverse participation ratio

$$IPR(\psi_j) = N \sum_{i=1}^{N} a_i^{k4} / \left(\sum_{i=1}^{N} a_i^{k2} \right)^2$$

(where $\psi_k = \Sigma_{i=1}{}^{N} a_i{}^{k} \phi_i$ is the k^{th} eigenstate and N is the number of atoms) analysis given in Fig. 7, one can see that there are defect states near Fermi level and no clear band gap is presented for the amorphous network. Note that the electron states near Fermi level do not have high IPR, suggesting that they are not strongly localized and that the amorphous model shows a metallic character. To have more information about the electronic structure, we also compute projected density of states. For both forms of BAs, As-p states play key roles near the Fermi level as seen in Fig. 6. B-p states have some contribution to the valance band as well. The band around −15 eV is mainly due to As-s states.

4. Discussion

The structural examinations reveal that the short-range order of

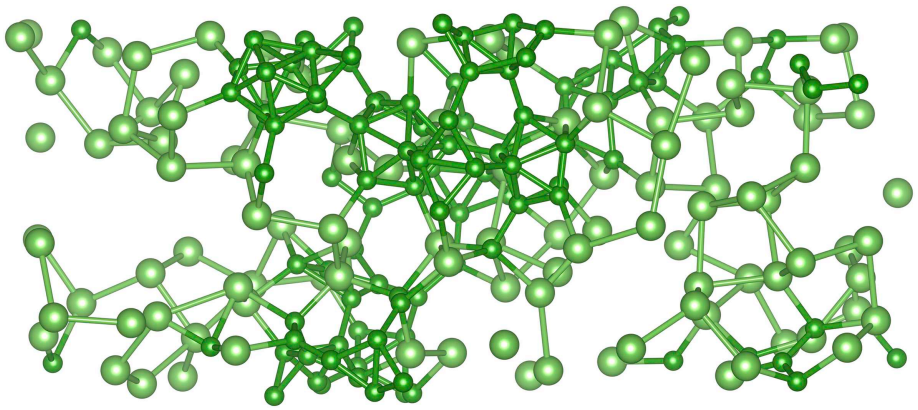

Fig. 3. Ball-stick representation of BAs amorphous model.

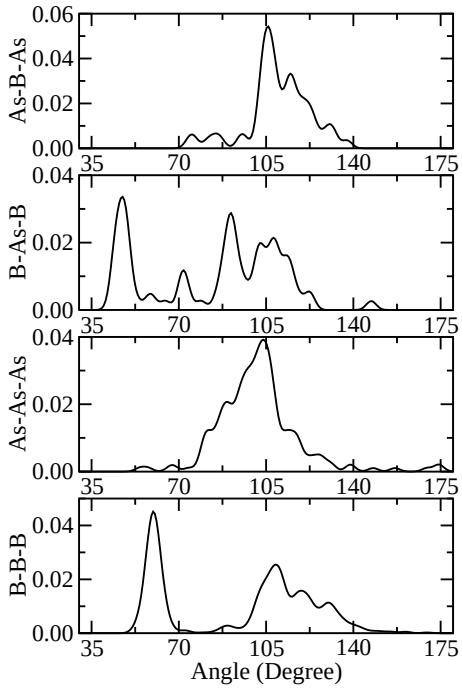

Fig. 5. Bond angle distribution functions.

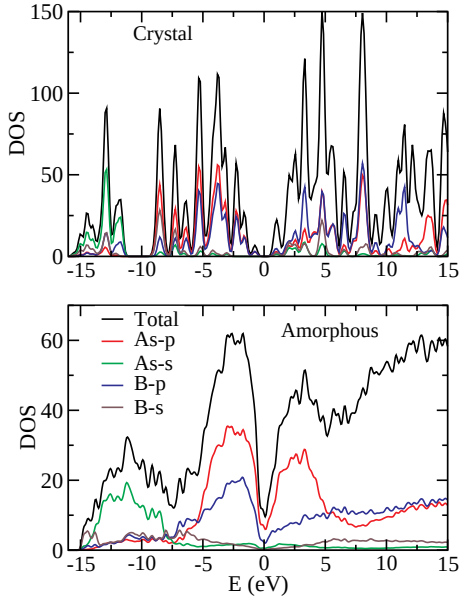

Fig. 6. Total and partial density of states of the crystalline and amorphous phases. The same line colorings are used for both structures.

amorphous BAs considerably is different from that of the ZB crystal. The amorphous model presents B-rich and As-rich domains and hence it shows strong chemical disorder. Its low iconicity is probably responsible for such a feature. B atoms have a tendency to form higher coordinated motifs, in particular, pentagonal pyramidal-like configurations as regularly seen in B and B-rich materials. Therefore the B-rich domains in the network exhibit some similarities with amorphous B. However, the key structures i.e., B_{12} molecules do not develop in our amorphous BAs configuration but a cage-like B_{10} cluster does during the solidification. To best of our knowledge, the formation of the B_{10} molecule has not been revealed in any boron based amorphous/crystalline materials. Yet the cage like B_{10} molecule, similar to one formed in our model, is not unfamiliar to researchers and can be stabilized by

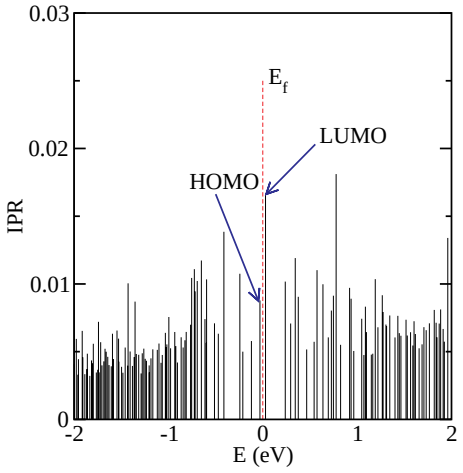

Fig. 7. Inverse participation ratio.

hydrogen. The properties and fabrication of the cage-like $B_{10}H_{10}$ cluster have been reported in the literature [44–47]. For the case of As atoms, they have a tendency to form a lower coordinated clusters with respective to the crystal. Actually As-rich regions show some resemblances with amorphous As.

The atomic volume of the noncrystalline state is 18.96 $Å^3$/atom, which is about 31% higher than 14.44 $Å^3$/atom in the crystal. So one see that amorphization yields a drastic volume swelling in BAs. The occurrence of lower coordinated chain-like structured As-atoms possibly drives a large volume expansion in the system (see Fig. 3).

When the electronic structure is considered, the amorphous form is metal in contrast to the crystal. This might be anticipated because the model consists of B-rich and As-rich domains and the crystalline and amorphous As are semimetal. Note that As-p states mainly control the electronic structure of the amorphous network.

5. Conclusions

We report the atomic structure and electrical properties of amorphous BAs by using first principles MD simulations. The BAs melt is rapidly solidified to generate an amorphous configuration. The formation of B-rich and As-rich domains is witnessed in the network. B atoms have a tendency to form higher coordinated motifs, relative to the crystal and its mean coordination is 4.97. The pentagonal pyramidal-like polyhedrons develop in the B-rich regions. The formation of B_{10} molecules is observed in the network. On the other hand, As-atoms attain lower coordinated configurations and its average coordination is 3.34. As atoms form chain-like structures and four-membered rings. All these observations reveal that the short-range order of the noncrystalline network is considerably different than that of the crystal. The amorphous form of BAs presents a metallic character.

Acknowledgements

This work was supported by the Abdullah Gül University Support Foundation. The calculations were partially run on TÜBİTAK ULAKBİM, High Performance and Grid Computing Center (TRUBA resources).

Declaration of Competing Interest

The authors declare that they have no competing financial interests.

References

[1] J.A. Perri, S. La Placa, B. Post, Acta Cryst 11 (1958) 310.
[2] J.C. Phillips, Bonds and Bands in Semiconductors, Academic Press, New York, 1973.

[3] R.M. Wentzcovitch, M.L. Cohen, P.K. Lam, Phys. Rev. B 36 (1987) 6058.
[4] J.S. Kang, M. Li, H. Wu, H. Nguyen, Y. Hu, Science 361 (2018) 575.
[5] S. Wang, S.F. Swingle, H. Ye, F.-R.F. Fan, A.H. Cowley, A.J. Bard, J. Am. Chem. Soc. 134 (2012) 11056.
[6] A. Zaoui, F.E. Hassan, J. Phys. Condens. Matter 13 (2001) 253.
[7] M.J. Herrera-Cabrera, P. Rodríguez-Hernández, A. Munoz, Int. J. Quantum Chem. 91 (2003) 191.
[8] H. Meradji, S. Drablia, S. Ghemid, H. Belkhir, B. Bouhafs, A. Tadjer, Phy. Status Solidi B 241 (2004) 2881.
[9] F.E. Hassan, H. Akbarzadeh, M. Zoaeter, J. Phys.: Condens. Matter 16 (2004) 293.
[10] N. Chimot, J. Even, H. Folliot, S. Loualiche, Physica B 364 (2005) 263.
[11] T. Azuhata, T. Sota, K. Suzuki, J. Phys. Condens. Matter 8 (1996) 3111.
[12] B. Bouhafs, H. Aourag, M. Certier, J. Phys. Condens. Matter 12 (2000) 5655.
[13] S.Q. Wang, H.Q. Ye, Phys. Rev. B 66 (2002) 235111.
[14] G.L. Hart, A. Zunger, Phys. Rev. B 62 (2000) 13522.
[15] D. Touat, M. Ferhat, A. Zaoui, J. Phys. Condens. Matter 18 (2006) 3647.
[16] S. Cui, W. Feng, H. Hu, Z. Feng, Y. Wang, Comput. Mater. Sci. 44 (2009) 1386.
[17] R. Ahmed, S.J. Hashemifar, H. Akbarzadeh, M. Ahmed, Comput. Mater. Sci. 39 (2007) 580.
[18] D.J. Stukel, Phys. Rev. B 1 (1970) 3458.
[19] A. Zaoui, S. Kacimi, A. Yakoubi, B. Abbar, B. Bouhafs, Physica B 367 (2005) 195.
[20] M. Sarwan, P. Bhardwaj, S. Singh, Chem. Phys. 426 (2013) 1.
[21] A. Boudjemline, M.M. Islam, L. Louail, B. Diawara, Physica B 406 (2011) 4272.
[22] R.G. Greene, H. Luo, A.L. Ruoff, S.S. Trail, F.J. DiSalvo Jr., Phys. Rev. Lett. 73 (1994) 2476.
[23] T.L. Chu, A.E. Hyslop, J. Electrochem. Soc. 121 (1974) 412.
[24] P. Ordejón, E. Artacho, J.M. Soler, Phys. Rev. B 53 (1996) R10441.
[25] N. Troullier, J.L. Martins, Phys. Rev. B 43 (1991) 1993.
[26] A.D. Becke, Phys. Rev. A 38 (1988) 3098.
[27] C. Lee, W. Yang, R.G. Parr, Phys. Rev. B 37 (1988) 37785.
[28] S. Le Roux, V. Petkov, J. Appl. Crystallogr. 43 (2010) 181.
[29] K. Momma, F. Izumi, J. Appl. Crystallogr. 44 (2011) 1272.
[30] R.G. Delaplane, T. Lundstrom, U. Dahlborg, W.S. Howells, Boron-Rich Solids, AIP Conf. Proc. 231 (1991), p. 241.
[31] R. Naslain, V.I. Matkovich (Ed.), Boron and Refractory Borides, Springer-Verlag, New York, 1977.
[32] S. Krishnan, S. Ansell, J.J. Felten, K.J. Volin, D.L. Price, Structure of liquid boron, Phys. Rev. Lett. 81 (1998) 586.
[33] H. Krebs, J. Non-Cryst. Solids 1 (1969) 455.
[34] R. Bellissent, G. Tourand, Journal de Physique 37 (1976) 423.
[35] A. Chiba, M. Tomomasa, T. Hayakawa, S.M. Bennington, A.C. Hannon, K. Tsuji, Phys. Rev. B 80 (2009) 060201.
[36] S.M. Ku, J. Electrochem. Soc. 113 (1966) 813.
[37] T.L. Chu, A.E. Hyslop, J. Appl. Phys. 43 (1972) 276.
[38] J.L. Lyons, J.B. Varley, E.R. Glaser, J.A. Freitas Jr., J.C. Culbertson, F. Tian, G.A. Gamage, H. Sun, H. Ziyaee, Z. Ren, Appl. Phys. Lett. 113 (2018) 251902.
[39] Q. Zheng, C.A. Polanco, M.H. Du, L.R. Lindsay, M. Chi, J. Yan, B.C. Sales, Phys. Rev. Lett. 121 (2018) 105901.
[40] I.H. Nwigboji, Y. Malozovsky, L. Franklin, D. Bagayoko, J. Appl. Phys. 120 (2016) 145701.
[41] M.P. Surh, S.G. Louie, M.L. Cohen, Phys. Rev. B 43 (1991) 9126.
[42] K. Bushick, K. Mengle, N. Sanders, E. Kioupakis, Appl. Phys. Lett. 114 (2019) 022101.
[43] J. Buckeridge, D.O. Scanlon, Phys. Rev. Mater. 3 (2019) 051601.
[44] W.H. Knoth, H.C. Miller, J.C. Sauer, J.H. Balthis, Y.T. Chia, E.L. Muetterties, Inorg. Chem. 3 (1964) 159.
[45] V.V. Avdeeva, A.V. Vologzhanina, L.V. Goeva, E.A. Malinina, N.T. Kuznetsov, Inorg. Chim. Acta 428 (2015) 154.
[46] A.P. Zhdanov, V.M. Retivov, G.A. Razgonyaeva, K.Y. Zhizhin, N.T. Kuznetsov, Russ. J. Inorg. Chem. 60 (2015) 771.
[47] K.Y. Zhizhin, A.P. Zhdanov, N.T. Kuznetsov, Russ. J. Inorg. Chem. 55 (2010) 2089.